An experimental rheological phase diagram of a tri-block co-polymer in water validated against dissipative particle dynamics simulations

Experimental rheological phase diagram of tri-block co-polymer in water validated against Dissipative Particle Dynamics simulations

Rossana Pasquino [1,], Hermes Droghetti[2], Paola Carbone[3], Shadi Mirzaagha[1], Nino Grizzuti[1], Daniele Marchisio[2]*

[1]Department of Chemical, Materials and Industrial Production, Università degli Studi di Napoli Federico II, P.le Tecchio 80, 80125 Napoli, Italy

[2]Department of Applied Science and Technology, Institute of Chemical Engineering, Politecnico di Torino, C.so Duca degli Abruzzi 24, 10129 Torino, Italy

[3]School of Chemical Engineering and Analytical Science, The University of Manchester, Oxford Road, Manchester M13 9PL, United Kingdom

Abstract:

Aqueous solutions of tri-block co-polymer surfactants are able to aggregate into a rich variety of microstructures, which can exhibit different rheological behavior. In this work, we study the diversity of structures detected in aqueous solutions of Pluronic L64 at various concentrations and temperatures by experimental rheometry and dissipative particle dynamics (DPD) simulations. Mixtures of Pluronic L64 in water (ranging from 0% to 90%wt of Pluronic L64) have been studied in both linear and non-linear regimes by oscillatory and steady shear flow. The measurements allowed for the determination of a complete rheological phase diagram of the Pluronic L64-water system. Linear and non-linear regimes have been compared to equilibrium and non-equilibrium DPD bulk simulations of similar systems obtained by using the software LAMMPS. The molecular results are capable of reproducing the equilibrium structures, which are in complete agreement with the ones predicted through experimental linear rheology. Simulations depict also micellar microstructures at long times when a strong flow is applied. These structures are directly compared, from a qualitative point of view, with the corresponding experimental results and differences between equilibrium and non-equilibrium phase diagrams are highlighted, proving the capability of detecting morphological changes caused by deformation in both experiments and DPD simulations. The effect of the temperature on the rheology of the systems has been eventually investigated and compared with the already existing non rheological phase diagram.

Introduction

Mixtures of amphiphilic surfactants and water are able to produce a rich variety of microstructures, ranging from spherical and cylindrical micelles, to hexagonal and lamellar structures [1]. In a system composed by different immiscible compounds and surfactants, phase diagrams can be built to identify the boundaries between the different phases [2]. The experimental derivation of a phase diagram is a quite standard procedure in this research area, although different techniques can bring to various and often contradicting results [2,3].

In the vast class of molecules having hydrophobic and hydrophilic moieties in the same structure, Pluronic® (or poloxamers) are a class of polymer-based systems built up by a sequence polyethylene oxide (PEO)-polypropylene oxide (PPO)-polyethylene oxide (PEO). They are a registered trademark of BASF corporation, firstly synthesized at the beginning of the 70s. This nonionic co-polymer can be manufactured varying the number of EO and PO monomers, such that the length of the hydrophilic (PEO) and hydrophobic (PPO) blocks can be varied to tune its amphiphilic properties, hence its temperature-dependent phase diagram [4]. Pluronics find various applications in detergency, foaming, dispersion stabilization, emulsification, pharmaceutics [4-6]. Due to their wide range of applications, they have been extensively studied in literature [7-20]. They have the capability, as well as surfactants, to form micelles in aqueous solutions. Pluronic micelles, however, differ from those formed by typical small-molecule surfactants in that the hydrophilic and hydrophobic groups are polymer chain segments. In addition, Pluronics show two hydrophilic “tails” and one hydrophobic core. They are also analogous to classical thermoplastic tri-block polymers, although with much lower molecular weights. They have, finally, analogies with a class of associating polymers, the telechelic polymers [21], which are linear chains containing associating “sticker” groups only at chain ends (i.e. the sticker being the PPO block in the Pluronic molecule).

Over the past decade, many studies were devoted to the properties of poloxamers in aqueous solution and the phase diagram of various Pluronic molecules (named with different labels based on the length of the repeating units, such as P84, L64, F127, P123) have been investigated [4, 8, 22-25].

At low temperature and very low concentrations, poloxamers exist as unimers. Micellization occurs while increasing the temperature or polymer concentration. The middle PPO block forms the core and the PEO blocks the corona, and a Critical Micellar Concentration (CMC) and Temperature (CMT) can be defined [26-29] for the different species. As the temperature increases, PPO tends to become less hydrophilic faster than PEO, and the co-polymers assume surfactant properties.

The phase diagram at equilibrium for the system L64/water, which is the system studied in the current work, has been previously derived by using nuclear magnetic resonance and X-ray scattering. By tuning temperature and concentration, it is possible to encounter different morphologies and in particular L_1 (micellar), H (hexagonal), L_α (lamellar), and L_2 (reverse micellar) [4].

Non-Newtonian behavior can be observed in water-poloxamer solutions at high surfactant concentration, while Newtonian behavior is obtained at lower concentrations. Phase transitions, changes in orientation, deformation and coalescence of micelles are examples of the phenomena involved when these fluids are subjected to shear [4, 30-32]. The transition from spherical to cylindrical or worm/rod-like micelles is also a very common event. These elongated structures can create a structured network or align themselves according to the direction of flow, thus determining a non-Newtonian behaviour. At higher concentration, the effect of the shear on complex systems plays an even more relevant role. For example, Gentile *et al* demonstrated that lamellar phases could rearrange their shape producing multilamellar vesicles, with a resulting non-Newtonian behavior [33]. When shear stresses act on these systems, the fate of equilibrium microstructures is yet difficult to infer from experimental measurements only. This becomes the perfect playground for computer simulations, along with more sophisticated techniques, such as SAXS or SANS, often used coupled to rheology. Microscopic models that are capable of reproducing molecular interactions can be used for such purpose, but self-assembly of large surfactant molecules, as well as the effect of shear on the observed microstructures, take place on timescales, which are commonly not accessible by traditional All-Atom Molecular Dynamics (AAMD). Therefore, mesoscopic models, such as Dissipative Particle Dynamics (DPD), can be used as a valid alternative to investigate wider timescales and predict

peculiar behaviors of such fluids, despite the molecular resolution is lost [34]. DPD describes the interaction between beads, representative of clusters of atoms and molecules, using a bead-spring model, repulsive soft potentials combined with stochastic and dissipative forces. Prhashanna *et al*, Cheng *et al*, Zhen *et al*, Cao *et al*, Li *et al* already discussed and validated the reliability of DPD to predict the formation of micelles, at thermodynamic equilibrium, and microstructures in systems composed by water and surfactants [34-38]. When a mechanical perturbation is applied (such as for example during a rheological experiment) shear stresses induce the deformation of the microstructure that can lead to phase transitions [33,39-41].

This work aims at investigating the role of concentration and temperature on the rheological response of aqueous solutions of Pluronic L64 (shortly L64) via both rheology experiments and DPD simulations. The first part of the paper will be devoted to the equilibrium properties. A rheological phase diagram will be built, which compares the rheological properties with the observed morphologies quantified via a cluster analysis, able to count and identify the geometry of the polymer structures via DPD simulations. The non-linear properties will be also investigated and the effect of temperature and concentration discussed.

Materials and methods

Pluronic L64 is the tri-block co-polymer investigated in this work. It has the formula: $((PEO)_{13}(PPO)_{30}(PEO)_{13})$, where PEO means polyethylene oxide and PPO is polypropylene oxide. The average molecular weight is 2900 g/mol and about 40% is composed by PEO. Mixtures of Pluronic L64 in water were investigated over a broad range of concentrations, ranging from 5% to 90% by weight. Experiments were performed at 20°, 30° and 50°C, whereas simulations were performed only at 20°C. A summary of the performed experiments and simulations is reported in Figure 1 (elaborated from Figure 2b of ref. [4]). Blue symbols specify the samples analyzed in this work experimentally, whereas red symbols indicate samples analyzed both with experiments and simulations.

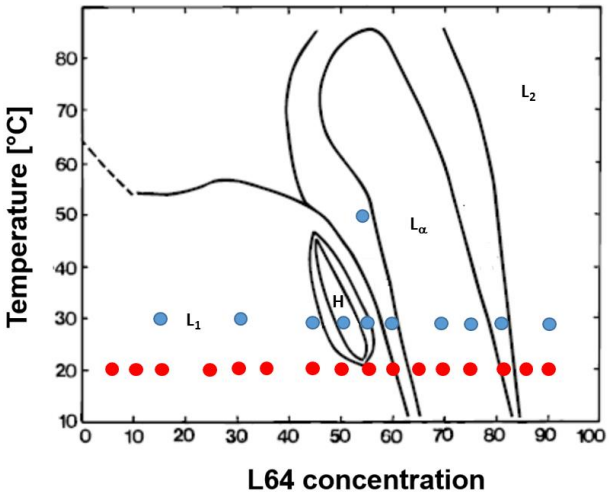

Figure 1. Phase diagram of Pluronic L64 in water (elaboration of Figure 2b from ref [4]). Blue symbols indicate the samples analyzed in this work experimentally, whereas red symbols indicate the samples analyzed via experiments and simulations. L_1: micellar phase, H: hexagonal phase, L_α: lamellar phase, L_2: reverse micellar phase.

Experiments: Pluronic L64 was purchased from Sigma Aldrich and was used without further purification. Rheological experiments were performed by a stress controlled rotational rheometer (MCR 702 TwinDrive, Anton Paar, Physica) equipped with an anti-evaporation tool. Steady shear and dynamic tests were performed using cone-plate geometries (50 and 25 mm diameter, both with 0.99° cone angle). The temperature was kept constant at the desired value by means of a Peltier unit. Flow curves were obtained in a range of shear rates between 100 and 10^{-5} s^{-1}. The sampling time was taken in a log scale fashion, starting from a few seconds at the highest shear rates and increasing the waiting time for the lowest values. Reproducibility was checked by tuning the measuring time during the flow curve and by performing the same tests with different fresh sample loadings. Frequency sweeps were performed in the range 100-0.1 rad/s in the linear regime (at low strain values, different according to the specific sample given the wide range of concentrations, and always lower than 5%).

Simulations: DPD is a coarse-grained model in which atoms and molecules are grouped together into clusters or beads, following the Langevin equation of motion and interacting through conservative, dissipative and stochastic forces [42-45]. The number of monomers clustered into one bead is 4.3 for the ethylene oxide repeated units and 3.3 for the propylene oxide repeated units, resulting into 15 beads for a Pluronic L64 chain (i.e. $A_3B_9A_3$, where A stands for the coarse-grained bead for ethylene

oxide and B for propylene oxide). Three water molecules are clustered together into a single bead of type C. Conservative forces include bonded interactions for beads belonging to the same chain/molecules, calculated with a harmonic potential, and non-bonded interactions, representing interactions between beads of different species, calculated with a soft potential. Dissipative and stochastic forces represent the coarse-grained degrees of freedom, through thermal noise and viscous dissipations, and are reconciled via the fluctuation-dissipation theorem, to respect the overall momentum balance. DPD simulations were carried out in LAMMPS on a cubic simulation box with periodic boundary conditions, while graphical outputs were produced using Ovito (Open Visualization Tool). For a selected set of operating conditions shear was applied to the simulation box by using the Lees-Edwards boundary conditions, mimicking what happens in dynamical rheological experiments. It is worth mentioning however that in order to overcome thermal noise and observe appreciable effects in reasonable time intervals, the shear applied can be incredibly large (up to 10^{11} s^{-1}) and, of course, not comparable to real experiments. Results of this part should be therefore considered *qualitative*. More details on the simulations can be found in a previous publication [46]. Simulations were performed on a cluster InfiniBand 4 TFLOPS on 10 cores AMD Bulldozer and 128GB of RAM.

Results and discussion

Rheological phase diagram: Figure 2 shows the linear viscoelastic response for various concentrations of the L64 solutions at 20°C. Figure 3 reports snapshots of DPD simulations of the same concentrations, at equilibrium conditions (i.e. absence of shear).

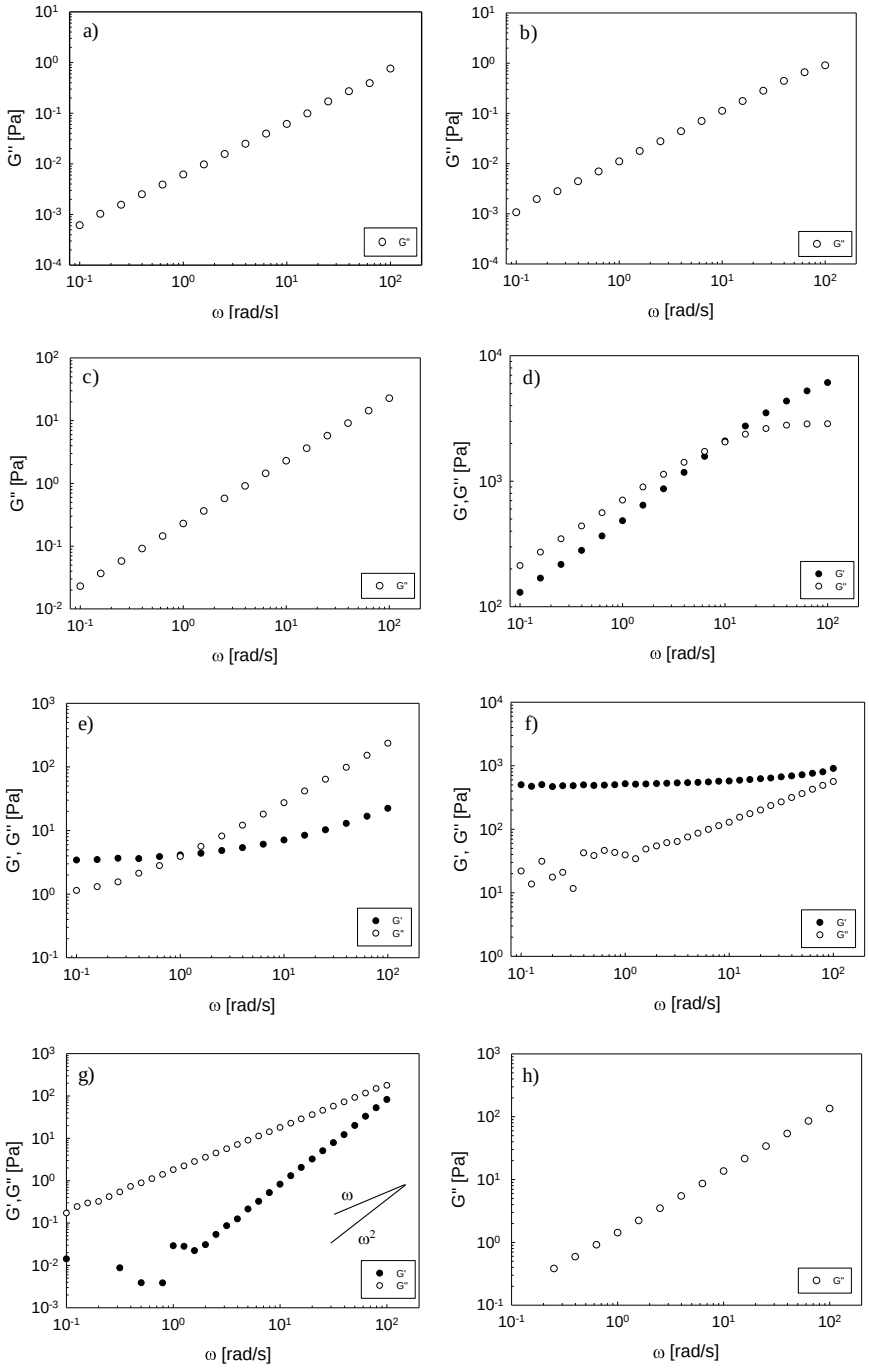

Figure 2. Linear viscoelasticity of Pluronic L64 in water at 20°C: a) 5% *wt* b) 25% *wt* c) 45% *wt* d) 55% *wt* e) 70% *wt* f) 75% *wt* g) 85% *wt* h) 90% *wt.* In g), terminal slopes are drawn.

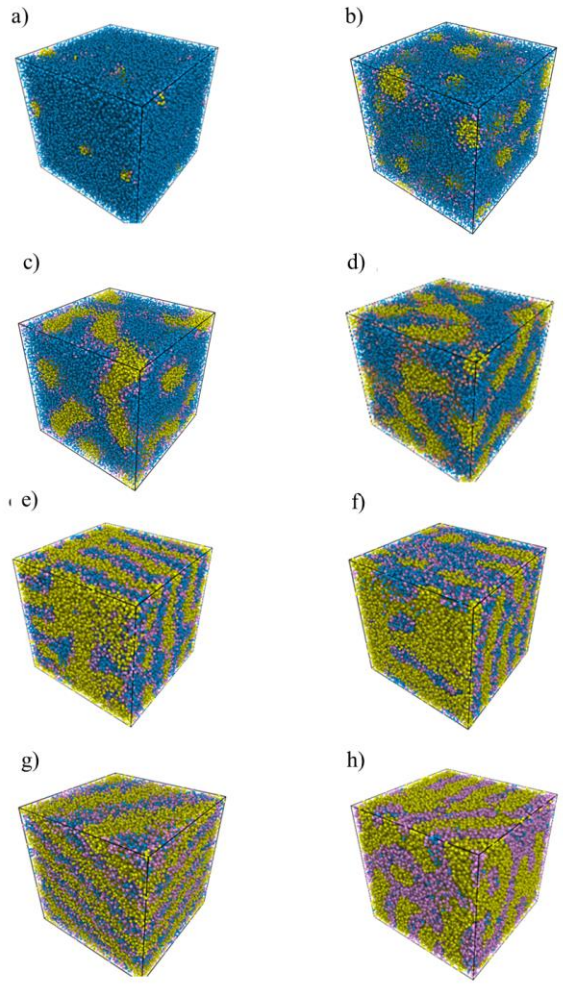

Figure 3. Snapshots of Pluronic L64 in water at different weight concentrations: a) 5% *wt* b) 25% *wt* c) 45% *wt* d) 55% *wt* e) 70% *wt* f) 75% *wt* g) 85% *wt* h) 90% *wt* at equilibrium, obtained with DPD simulations. In each snapshot, a full view comprising water (blue), PEO (pink) and PPO (yellow) beads is reported.

At very low Pluronic concentrations (see for example 5%*wt*, Figure 2a), only the viscous modulus is detected with a terminal slope of one, maintained in the whole frequency range, with no hint of elasticity. This suggests that Pluronic molecules self-assemble in spherical micelles, as confirmed by Figures 3a, which shows the simulated microstructure, clearly spherical, at the same concentration under no shear. In figure 3a it is possible to observe that PPO cores (yellow beads) of different Pluronic L64 molecules come close enough to induce aggregation, and exposing their PEO tails (pink beads) to the water environment (blue beads). Almost no unimers are present in the simulation box, confirming that the concentration of Pluronic L64 is above the CMC, as proven by the phase diagram in Figure 1.

For higher Pluronic concentrations, the viscous modulus increases (Figures 2b and 2c), due to the increase in the number density of spherical micelles (Figures 3b and 3c), but no elasticity can be measured. Figure 2d shows the viscoelastic response for the 55%*wt* sample, with elastic and viscous moduli now of the same order of magnitude, and a well-defined cross-over frequency, whose inverse can be considered as a relaxation time for the arising rod/wormlike micellar structure. Figure 3d confirms that, at 55%*wt*, spherical micelles are definitely replaced by a more complicated structure, obtained from the connection between non-spherical elongated aggregates, similar to rod/wormlike chains.

At a concentration of 70%*wt* the viscoelasticity changes completely (see Figure 2e), showing the fingerprint of a soft solid-like system, with a plateau at low frequencies, which can be considered as a hint of a structured system, and a characteristic time given by the cross-over between the viscoelastic moduli. Snapshots of figure 3e clearly show the transition from a completely disordered system observed at 55% *wt,* to a more ordered one, at 70%*wt*. In this regime, lamellae can be already appreciated. Lamellae are composed by aligned sheets of Pluronic L64 (chains are now oriented) alternated to water layers.

Figure 2f shows the viscoelastic response of a fully soft-solid sample (at 75%*wt*), with an elastic modulus overcoming the viscous one in the whole range of frequencies, which translates again in fully ordered lamellar phase in the simulation (see Figure 3f), similar to what observed for the previously discussed concentration.

At 85%*wt* (Figure 2g) the system shows the typical response of a viscoelastic fluid with terminal slopes for G' and G'', corresponding to the microstructures observed in Figure 3g.

At concentration higher than 85%*wt* the solutions return to be purely viscous, although with G" significantly higher than those measured at very low Pluronic concentrations (Figure 2h). This corresponds to a microstructure of reverse micelles, where a continuous phase of Pluronic L64 is achieved and water molecules are entrapped in L64 spherical micelles. In figure 3h, it is possible to see just few water beads surrounded by disordered chains of Pluronic L64.

For a better comprehension of the morphological transitions arising with increasing concentration at equilibrium conditions, animation files coming out from DPD simulations, with water beads and making water beads invisible, are added in *Supporting Information* for two Pluronic concentrations (5% and 55%).

The effect of temperature has been also investigated by experiments [47]. Simulations in this case have not been performed because the interaction parameters were validated in a range of temperature lower than the one selected for the experimental tests. In DPD, the concept of temperature is not straightforward. Also, the set of conservative parameters has been retrieved to reproduce the equilibrium configuration at room temperature for the Pluronic L64 / water mixture. Figure 4.a shows the viscoelastic response for the 55%*wt* sample at 50°C and Figure 4.b the viscoelastic response during a temperature ramp from 5°C to 80°C at 1 rad/s, 0.1% of strain and 2°C/min. The 55%*wt* sample at 50°C shows the fingerprint of a lamellar phase, in agreement with the phase diagram [4,33]. During the thermal ramp, the microstructural changes, taking place as a function of temperature, are clearly visible. The non-monotonic changes of the moduli closely follow the temperature-induced phase transitions of the phase diagram, as highlighted by the vertical lines of Figure 4.b, which correspond to the phase transition curves of Figure 1 [4].

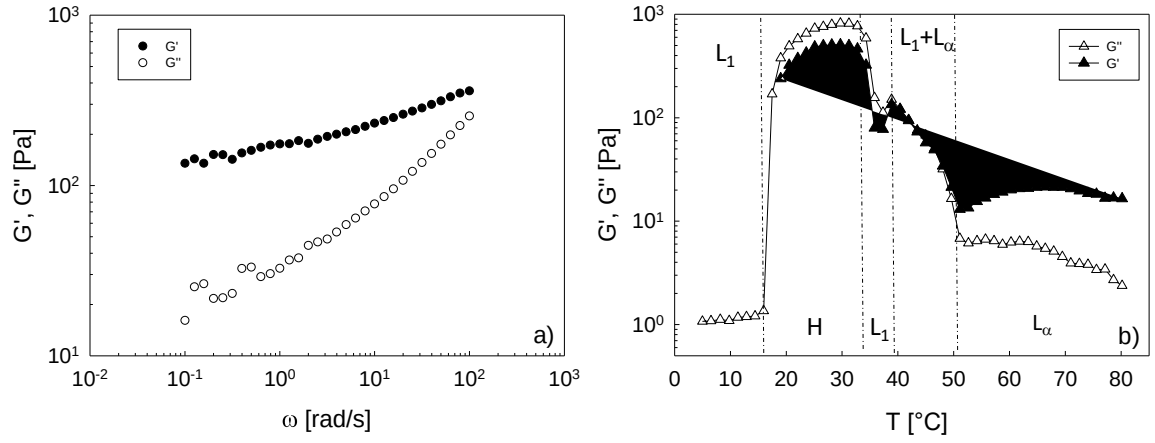

Figure 4. a) Viscoelastic response at 50°C for the sample with L64 at 55%w; b) Viscoelastic moduli on the same sample as function of temperature during a temperature ramp performed at 2°C/min, 1 rad/s, 0.1% strain. The vertical broken lines correspond to the phase transitions as obtained from Figure 1. L_1: micellar phase; H: hexagonal phase; L_α: lamellar phase.

To summarize all the linear viscoelasticity results, the complex viscosity is plotted in Figure 5 at 20° and 30°C as a function of L64 concentration. The viscosity trend resembles the phase diagram shown in Figure 1 and the non-monotonic behavior again depicts the various morphological transitions. At very low concentrations, L64 assembles in spherical micelles, which do not contribute significantly to the viscosity. At a specific concentration, which is lower for higher temperatures, due to the enhanced hydrophobicity of the polypropylene oxide blocks, the viscosity abruptly increases by orders of magnitude, marking a net morphological transition, and still remaining in the micellar phase, from spherical to rod/wormlike micelles. The sharp increase in viscosity (almost three orders of magnitude) at 20°C highlights the presence of long entangled micelles (see Figure 2b) whereas at 30°C the high viscosity value corresponds to a hexagonal phase, well depicted in Figure 1. The non-monotonic "breathing" of the viscosity after the first region of high viscosity level falls in a region of the phase diagram that relates with planar lamellar phase L_α, characterized by flat and multiple bilayers stacked in one-dimensional order [33]. With increasing concentration, possibly, either the bilayer bending rigidity changes or bicontinuous phases may occur, which in turn influence the mechanical response [33,48]. Less interesting is the rheological response at very high L64 concentrations (above 85%*wt*), where reverse micelles occur, and a Newtonian behavior is recovered.

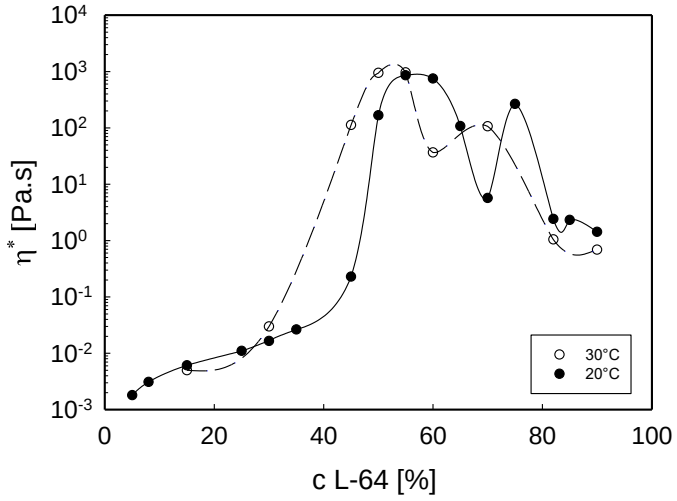

Figure 5. Complex viscosity evaluated at 1rad/s as function of the Pluronic L64 weight concentration. 20°C: black symbols; 30°C: empty circles. The lines are meant to guide the eye.

Flow curves and yield stress: Flow curves were performed on various samples at different concentrations and temperatures. Newtonian behavior was measured at low concentrations (below 45%*wt*). At higher concentrations, the solution responds as a viscoplastic fluid. One example of such a behavior is reported in Figure 6 for the 55%*wt* sample at 50°C. In Figure 6, the best fit of the experimental data with the Herschel–Bulkley model is also reported, which allows for the quantitative determination of the yield stress [49]. Figure 7 shows the comparison between steady and complex viscosity at 20°C, evaluated at $1s^{-1}$ and 1 rad/s, respectively. The inset in Figure 7 shows the complex viscosity for the sample at 75% along with its shear viscosity, measured at 20°C. Although it is clear that the non-linearity is more complex than what it can be shown at a fixed shear rate/frequency, Figure 7 gives a hint of the concentration region for which a strong external flow can induce significant rheological changes.

There is a good agreement between the rheological response in dynamic and steady modes for samples with a simple morphology (spherical and reverse micelles), whereas the Cox-Merz rule [50] does not held for samples with L64 concentration in the range 45-80%*wt*, which are characterized by a microstructure that can be strongly affected by flow. Consistently, the steady viscosity shows a lower viscosity value if compared to the corresponding one in dynamic response, indicating a structure development and/or intermolecular rearrangements in the non-linear regime.

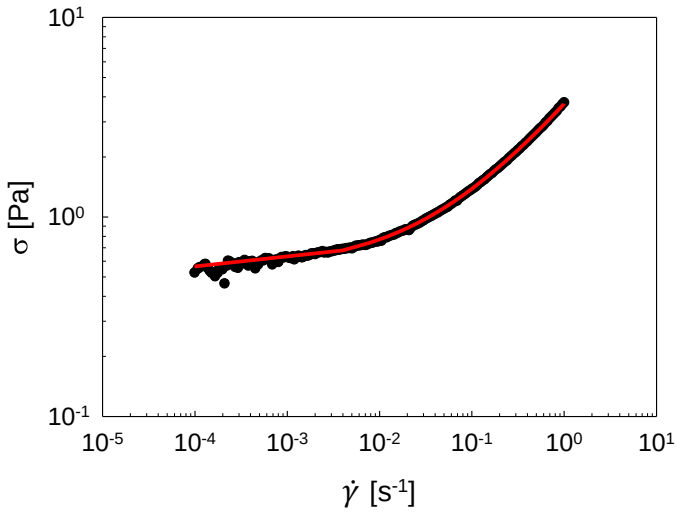

Figure 6. Shear stress *vs* shear rate for Pluronic L64 at 55%w and 50°C. Black data: experimental points. Red line is the best fit through data with the Herschel–Bulkley equation: $\sigma = \sigma_0 + k\dot{\gamma}^n$ (in SI units: $\sigma_0 = 0.55 \pm 0.003; k = 3.14 \pm 0.02; n = 0.57 \pm 0.004$).

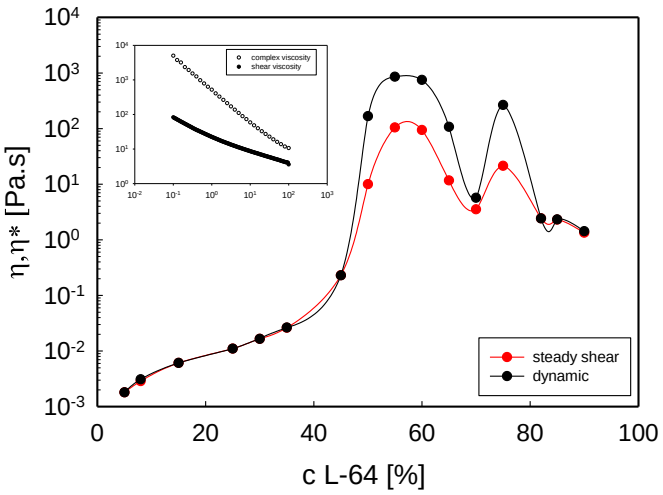

Figure 7. Viscosity evaluated at 1rad/s (black symbols) and $1s^{-1}$ (red symbols) as function of the L64 weight concentration at 20°C. Inset: shear (black symbols) and complex viscosity (empty symbols) in Pa.s as function of shear rate (s^{-1}) and angular frequency (rad/s) for the sample with L64 at 75%.

The experimental flow curves can be validated against simulations results. The simulations are performed at a fixed shear rate and the arising flow-induced microstructures at long times can be appreciated and compared with the rheological response. For very low L64 concentrations (up to 25% - see Figure 8a), simulations show that flow can induce shear-induced coalescence of small spherical micelles into larger ones. In other words, in this concentration range, the spherical shape of the new aggregates is not altered by such phenomenon, and the experimental viscosity at equilibrium conditions (in linear oscillatory response) overlaps on the shear viscosity (in non-linear steady response), thus proving that the number density of the micellar spheres does not affect significantly the rheological response.

As the L64 concentration increases, DPD simulations highlight flow-induced transitions. For example, Figure 8b) shows the shear structure at long times for the 55%*wt* sample. By comparing Figure 3d) with Figure 8b), a transition from a disordered interconnected structure to a more ordered hexagonal phase can be identified. Cylindrical structures are trapped in a more ordered configuration. In other words, in Figure 8b) elongated structures can be detected and easily counted, and they clearly

separate between each other. In Figures 8c, and 8d, at 70%*wt* and 75%*wt*, respectively, ordered lamellar phases in the flow direction were observed, whose orientation changes according to the shear imposed on the simulation box. However, no modification of the microstructure is observed in this regime. In Figure 8e a similar topological pattern, already identified in the equilibrium simulation, can be recognized. Again, sheets of Pluronic L64 alternate to water ones. A small bending of the sheets (or lamellae) can be appreciated but no substantial differences are highlighted. The number of lamellae does not change when moving between equilibrium and non-equilibrium configurations. Figure 8f shows the evolution of the disordered phase, recognized at equilibrium, into a more ordered pattern. The structure is again resembling lamellar phase, but in this case the amount of water is too small to create entire sheets of water between the chains. Water is instead trapped between the Pluronic L64 sheets. For a better comprehension of the combined effect of concentration and shear, DPD movies can be found in *Supporting Information*.

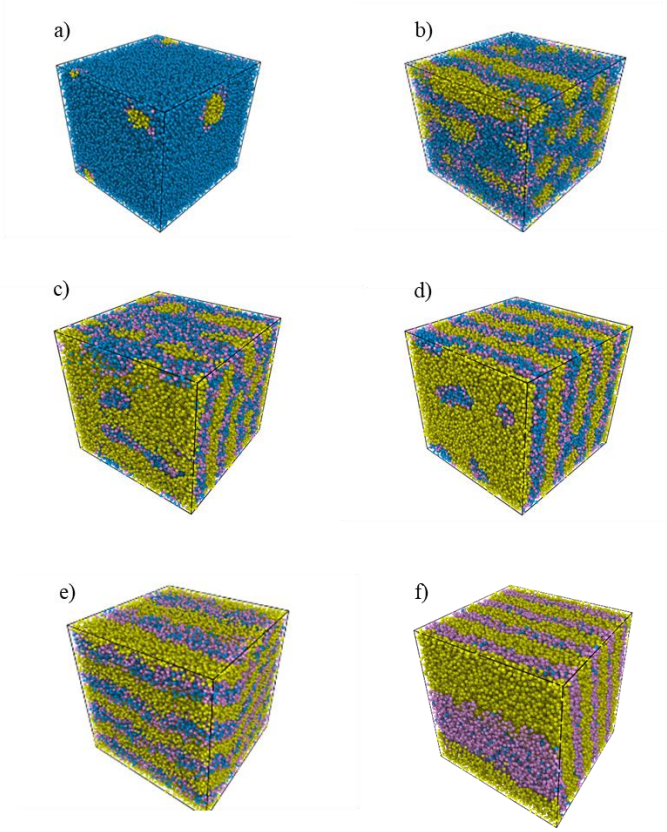

Figure 8. Snapshots of the non-equilibrium structure at long times for Pluronic L64 in water at different weight concentrations: 5% *wt*, 55% *wt*, 70% *wt,* 75% *wt*, 85% *wt*, 90% *wt.* In each snapshot, a full version comprising water (blue), PEO (pink) and PPO (yellow) beads is reported together with a lean version, where water was faded out for simplicity. The shear rate imposed on the system is equal to 0.1 DPD units.

Finally, Figure 9 shows the yield stress (see Figure 6 caption), as a function of L64 concentration at two different temperatures, 20 and 50°C, highlighting the concentration range in which flow has relevant effects. Figure 9 shows that samples with concentration lower than 50%*wt* do not show a solid-like behavior, as well as samples with concentration higher than 80%*wt*. The sample with a concentration of 55%*wt* shows a yield stress behavior at 50°C, but not at 20°C. In the range of measurable yield stress, the sample microstructure breaks up and the system can flow, if subjected to a sufficient stress. The dependence of the yield stress on concentration is more pronounced for the lowest temperature. Samples with a measurable yield stress exhibit a low-plateau elastic modulus in viscoelastic regime, which show the same trend with concentration but remarkably higher values in comparison to the yield stress.

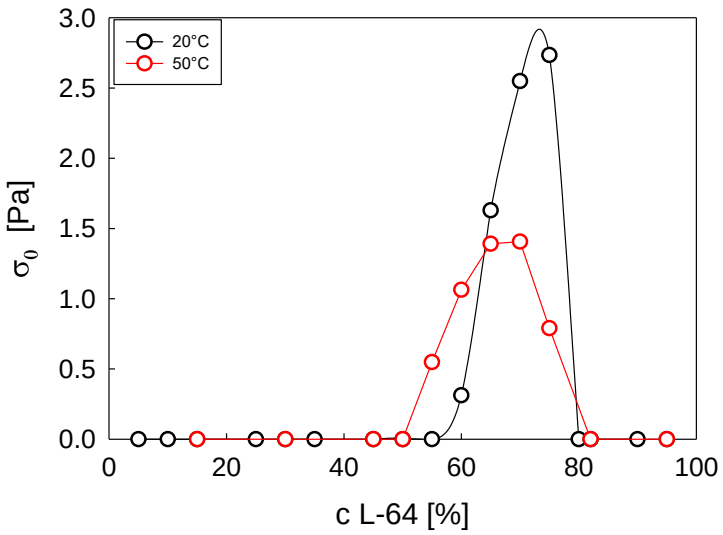

Figure 9. Yield stress value at 20°C and 50°C as function of L64 concentration.

Conclusions

The rheological results, also supported by DPD simulations, confirm the non-trivial behavior of the Pluronic L64 in water and clearly indicate the different morphologies explored by the system upon concentration changes. The linear viscoelastic response overlaps on the traditional phase diagram

obtained via scattering techniques [4] and proves that rheology and DPD simulations are able to track morphological transitions.

More specifically, under equilibrium conditions, i.e. in the absence of flow for DPD simulations and small amplitude oscillatory shear experiments, the results show that:

- at very low Pluronic concentrations, the polymer self-assembles in micellar phases (spherical or cylindrical) and the rheology is relatively trivial, displaying either a viscous or a liquid-like viscoelastic response with a characteristic relaxation time. The shape of the aggregates does not change, as it stays spherical or cylindrical based on the initial concentration;
- when the Pluronic concentration is in the range 65%<*wt*<80%, a lamellar phase arises, as proven by DPD snapshots at equilibrium [33];
- Eventually, when the concentration exceeds 90%*wt*, reverse micelles form, and a liquid-like behavior is recovered, with water trapped into the articulate molecular network originated by the Pluronic L64.

We also investigated, both experimentally and with DPD simulations, the effect of steady flow on the microstructure evolution of Pluronic L64 aggregates, for which no comparison ca be done with the available phase diagram:

- at very low and very high Pluronic L64 concentrations, where spherical structures characterize the morphology in equilibrium conditions, steady shear flow has no effect on the microstructure and spherical aggregates can be still recognized at long times. In this case, the rheological responses in dynamic and shear flow overlap, although the number of spherical micelles in the microstructure can change.
- in the intermediate concentration range, 55%<*wt*<75%, morphology changes due to shear strength, and elongated structures, as well as lamellas, can be aligned and stretched in the flow direction. This results in a flow-induced microstructure, different from the corresponding one at equilibrium, as proven by DPD simulations, and in a significantly lower shear viscosity if compared to the complex viscosity.

Acknowledgements

RP thanks R. Pascarella and S. De Lucia for their help with lab measurements. SM thanks UniNa for a fellowship program. Computational resources were provided by HPC@POLITO, a project of Academic Computing within the Department of Control and Computer Engineering at the Politecnico di Torino (http://www.hpc.polito.it).

References

[1] J. N. Israelachvili, D. J. Mitchell and B. W. Ninham, *Journal of the Chemical Society, Faraday Transactions 2: Molecular and Chemical Physics*, 1976, **72**, 1525-1568.

[2] R. Zana, *Advances in Colloid and Interface Science*, 1995, **57**, 1-64.

[3] L. Piculell, B. Lindman, Advances in Colloid and Interface Science, 1992, **41**, 149-178.

[4] D. Alexandridis, D. Zhou and A. Khan *Langmuir,* 1996, **12**, 2690-2700.

[5] I. R. Schmolka, *Am. Perfum. Cosmet.* 1967, **82**, 25-30.

[6] M. L. Adams, A. Lavasanifar and G.S. Kwon *J. Pharm. Sci.,* 2003, **92**, 1343-1355.

[7] A. V. Kabanov, E. V. Batrakova and V. Y. Alakhov, *J. Controlled Release,* 2002, **82**, 189-212.

[8] Y. Meng, D. Gu, F. Zhang, Y. Shi, L. Cheng, D. Feng, Z. Wu, Z. Chen, Y. Wan, A. Stein and D. Zhao, *Chem. Mater.*, 2006, **18**, 4447-4464.

[9] P. Holmqvist, P. Alexandridis and B. Lindman, *J. Phys. Chem. B*, 1998, **102**, 1149-1158.

[10] R. Ivanova, B. Lindman and P. Alexandridis, *Langmuir*, 2000, **16**, 9058-9069.

[11] B. Svensson, P. Alexandridis and U. Olsson, *J. Phys. Chem. B*, 1998, **102**, 7541-7548.

[12] D. Zhou, P. Alexandridis and A. Khan, *J. Colloid Interface Sci.*, 1996, **183**, 339-350.

[13] K. Aramaki, M. K. Hossain, C. Rodriguez, M. H. Uddin and H. Kunieda, *Macromolecules*, 2003, **36**, 9443-9450.

[14] V. Castelletto, P. Parras, I. W. Hamley, P. Bäverbäck, J. S. Pedersen and P. Panine, *Langmuir*, 2007, **23**, 6896-6902.

[15] F. Aydin, X. Chu, G. Uppaladadium, D. Devore, R. Goyal, N. S. Murthy, Z. Zhang, J. Kohn and M. Dutt, *J. Phys. Chem. B*, 2016, **120**, 3666-3676.

[16] T. Taddese and P. Carbone, *J. Phys. Chem. B*, 2017, **121**, 1601-1609.

[17] A. M. Zaki and P. Carbone, *Langmuir*, 2017, **33**, 13284-13294.

[18] S. Nawaz and P. Carbone, *J. Phys. Chem. B,* 2014, **118**, 1648-1659.

[19] S. Nawaz, M. Redhead, G. Mantovani, C. Alexander, C. Bosquillon and P. Carbone, *Soft Matter*, 2012, **8**, 6744-6754.

[20] X. Zhou, X. Wu, H. Wang, C. Liu and Z. Zhu, *Physical Review E* 2011, **83**, 041801-1-041801-5.

[21] M. A. Tasleden, M. U. Kahveci and Y. Yagci, *Progress in Polymer Science*, 2011, **36**, 455-567.

[22] S. Gaisford, A. E. Beezer and J. C. Mitchell, *Langmuir,* 1997, **13**, 2606-2607.

[23] T. Liu, V.M. Nace and B. Chu, *Langmuir,* 1999, **15**, 3109-3117.

[24] W. Batsberg, S. Nodni, C. Trandum and S. Hvidt, *Macromolecules,* 2004, **37**, 2965-2971.

[25] F. Artzner, S. Geiger, A. Olivier, C. Allais, S. Finet and F. Agnely, *Langmuir,* 2007, **23**, 5085-5092.

[26] B. Michels, G. Waton and R. Zana *Colloids Surf. A,* 1997, **13**, 3111-3118.

[27] P. Alexandridis, J. F. Holzwarth and T. A. Hatton, *Macromolecules,* 1994, **27**, 2414-2425.

[28] R. Wang, H. Knoll, F. Rittig and J. Karger, *Langmuir,* 2001, **17**, 7464-7467.

[29] W. Brown, K. Schillen, M. Almgren, S. Hvidt and P. Bahadur, *J. Phys. Chem.,* 1991, **95**, 1850-1858.

[30] W. Richtering, *Curr. Opin. Colloid Interface Sci.,* 2001, **6**, 446-450.

[31] K. Mortensen, *Curr. Opin. Colloid Interface Sci.*, 2001, **6**, 140-145.

[32] P. Butler, *Curr. Opin. Colloid Interface Sci.*, 1999, **4**, 214-221.

[33] L. Gentile, B. F. B. Silva, S. Balog, K. Mortensen and U. Olsson, *J. Colloid Interface Sci.,* 2012, **372**, 32-39.

[34] R. D. Groot and P. B. Warren, *J. Chem. Phys.*, 1997, **107**, 4423-4435.

[35] A. Prhashanna, S. A. Khan and S. B. Chen, *Colloids Surf. A Physicochem. Eng. Asp.,* 2016, **506**, 457-466.

[36] F. Cheng, X. Guan, H. Cao, T. Su, J. Cao and Y. Chen, *Int. J. Pharm.,* 2015, **492**, 152-160.

[37] X. Cao, G. Xu, Y. Li and Z. Zhang, *J. Phys. Chem. A,* 2005, **109**, 10418-10423.

[38] L. Zhen, K. Liu, D. Huang, X. Ren and R. Li, *J. Dispersion Sci. Technol.,* 2016, **37**, 941-948.

[39] Y. Li, H. Zhang, M. Bao and Q. Chen, *J. Dispersion Sci. Technol*., 2012, **33**, 1437-1443.

[40] S. C. Mehta, P. Somasundaran and R. Kulkarni, *J. Colloid Interface Sci.*, 2009, **333**, 635-640.

[41] V. M. Sadtler, M. Guely, P. Marchal and L. Choplin, *J. Colloid Interface Sci.*, 2004, **270**, 270-275.

[42] P. J. Hoogerbrugge, J. M. V. A Koelman, *Europhys Lett,* 1992, **19**, 155-160.

[43] P. Español and P. B. Warren, *Journal of Chemical Physics,* 2017, **146**, 150901-1 - 150901-16.

[44] I. Pagonabarraga and D. Frenkel, *J. Chem. Phys.*, 2001, **115**, 5015-5026.

[45] I. Pagonabarraga and D. Frenkel, *Mol. Simul.*, 2000, **25**, 167-175.

[46] H. Droghetti, I. Pagonabarraga, P. Carbone, P. Asinari and D. Marchisio, submitted to *J. Chem. Phys.*, 2018.

[47] L. Lobry, N. Micali, F. Mallamace, C. Liao, and S. H. Chen, *Phys. Rev. E,* 1999, **60**, 7076-7087.

[48] G. G. Chernik, *Curr. Opin. Colloid Interface Sci.,* 2000, **4**, 381-390.

[49] H. A. Barnes, *J. Non-Newtonian Fluid Mech.*, 1999, **81**, 133-178.

[50] W. P. Cox and E. H. Merz, *J Polym Sci,* 1958, **28**, 619-622.